

Adaptive cluster expansion approach for predicting the structure evolution of graphene oxide

Xi-Bo Li, Pan Guo, D. Wang, Yongsheng Zhang, and Li-Min Liu

Citation: [The Journal of Chemical Physics](#) **141**, 224703 (2014); doi: 10.1063/1.4903310

View online: <http://dx.doi.org/10.1063/1.4903310>

View Table of Contents: <http://scitation.aip.org/content/aip/journal/jcp/141/22?ver=pdfcov>

Published by the [AIP Publishing](#)

Articles you may be interested in

[First-principles studies on graphene-supported transition metal clusters](#)

J. Chem. Phys. **141**, 074707 (2014); 10.1063/1.4893328

[The electronic property of graphene adsorbed on the siloxane and silanol surface structures of SiO₂: A theoretical prediction](#)

Appl. Phys. Lett. **101**, 253107 (2012); 10.1063/1.4772494

[Doping of graphene adsorbed on the a-SiO₂ surface](#)

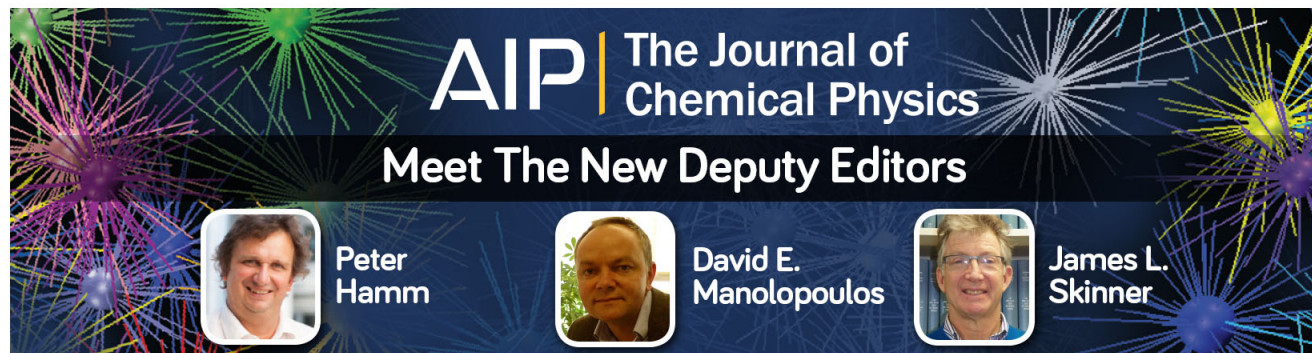
Appl. Phys. Lett. **99**, 163108 (2011); 10.1063/1.3653261

[Adsorption of nitrogen oxides on graphene and graphene oxides: Insights from density functional calculations](#)

J. Chem. Phys. **134**, 044710 (2011); 10.1063/1.3541249

[Greatly enhanced adsorption and catalytic activity of Au and Pt clusters on defective graphene](#)

J. Chem. Phys. **132**, 194704 (2010); 10.1063/1.3427246

A banner for AIP The Journal of Chemical Physics. It features the journal's logo at the top. Below the logo, the text 'Meet The New Deputy Editors' is displayed. Underneath this text are three circular portraits of the new deputy editors: Peter Hamm, David E. Manolopoulos, and James L. Skinner. The background of the banner is dark blue with abstract, colorful, starburst-like patterns in green, yellow, and purple.

Adaptive cluster expansion approach for predicting the structure evolution of graphene oxide

Xi-Bo Li,¹ Pan Guo,¹ D. Wang,¹ Yongsheng Zhang,² and Li-Min Liu^{1,a)}

¹Beijing Computational Science Research Center, Beijing 100084, China

²Key Laboratory of Materials Physics, Institute of Solid State Physics, Chinese Academy of Sciences, Hefei 230031, China

(Received 21 September 2014; accepted 21 November 2014; published online 9 December 2014)

An adaptive cluster expansion (CE) method is used to explore surface adsorption and growth processes. Unlike the traditional CE method, suitable effective cluster interaction (ECI) parameters are determined, and then the selected fixed number of ECIs is continually optimized to predict the stable configurations with gradual increase of adatom coverage. Comparing with traditional CE method, the efficiency of the adaptive CE method could be greatly enhanced. As an application, the adsorption and growth of oxygen atoms on one side of pristine graphene was carefully investigated using this method in combination with first-principles calculations. The calculated results successfully uncover the structural evolution of graphene oxide for the different numbers of oxygen adatoms on graphene. The aggregation behavior of the stable configurations for different oxygen adatom coverages is revealed for increasing coverages of oxygen atoms. As a targeted method, adaptive CE can also be applied to understand the evolution of other surface adsorption and growth processes. © 2014 AIP Publishing LLC. [<http://dx.doi.org/10.1063/1.4903310>]

I. INTRODUCTION

The unique mechanical,¹ structural,² electronic,^{3,4} and thermal properties⁵ of graphene have stimulated numerous studies since it was successfully extracted from graphite by Geim and Novoselov in 2004.² However, there is still a long way to go for the application of graphene in semiconductors because of the existence of a zero band-gap. Many groups have used different methods to control and modulate the electronic properties of graphene and other two-dimensional (2D) materials.^{6–16} Among these attempts, chemical functionalization^{6,9–13} of graphene is the most effective technique to tune the band-gap. Graphene oxide (GO) was first fabricated almost 150 years ago and the band-gap of GO strongly depends on the atomic structure of GO.^{12,13,17,18} In addition, GO is an important intermediate in the process of large-scale graphene production from graphite.^{19,20} In the process of graphene production, GO with different degrees of oxidation can be synthesized by the modified Hummers method and then exfoliated by ultrasonication.¹⁰ After the treatment, both sides of graphene are oxidized, and the ratio of O/C can reach a maximum value of nearly 1 and can be reversed by thermal reduction.^{12,13,21}

In the past few years, many experimental and theoretical studies have been carried out to establish a thorough understanding of the interaction of oxygen with bare graphene and the atomic structures of GO.^{12,13,21–38} Several advanced experimental techniques, such as nuclear magnetic resonance spectroscopy^{20,37,38} and atomic force microscopy,¹⁹ have been used to characterize the structure of GO. The experiments mainly reached a consensus: part of graphene was

oxidized and the other part was pristine graphene.¹⁷ On the theoretical side, many density functional theory (DFT) calculations have been performed to explore how graphene is oxidized to GO by oxygen atoms.^{22,25,27–30,32,35,36} Nguyen *et al.*³⁰ showed that the oxidation of graphene on both sides follows a 2D nucleation-and-growth mechanism with configurations favoring clusters with oxygen atoms occupying adjacent bridge sites. Topsakal *et al.*²⁸ found that GO prefers to form an inhomogeneous phase during the oxidation of graphene on one side. Recently, Huang *et al.*²⁹ suggested that well-ordered GO could be obtained at low oxygen coverage on one side of graphene, which could overcome phase inhomogeneity.

Because of the huge number of possible configurations even on the limited number of occupying sites, it is difficult to uncover the detailed oxidation progress of graphene by conventional theoretical methods. For one species of adatom, if all possible configurations of n atoms occupying all possible sites on a selected unit surface are considered, the number of configurations is large. For example, the possible number of configurations for 10 atoms distributed on 100 equivalent sites is nearly 10^{13} . Because the adsorption and growth processes are rather complex, empirical force fields cannot easily deal with these types of problems. Although in principle stable configurations can be obtained by first-principles calculations, the number of configurations is too large to handle in practice. Global optimization methods,^{39–41} although powerful in predicting new structures, are also unable to handle this type of problem. However, the cluster expansion (CE) approach based the Ising model is a possible way to solve this type of problem.^{42,43} In the CE approach, some of the configurations are first investigated by DFT calculations and the DFT energy of each configuration is expanded in series over

^{a)}E-mail: limin.liu@csrsc.ac.cn

discrete interactions (the effective cluster interactions (ECIs)) between the lattice sites. By selecting an appropriate number and appropriate values of the ECIs, the energies of configurations can be well-represented by the ECIs and are comparable to DFT calculated results. This could greatly reduce the computational cost while maintaining accuracy.

In this work, an adaptive CE approach combined with first-principles calculations is used to explore surface adsorption and growth processes. The ECI parameters are constructed and selected at a relatively low coverage of adatoms and then the selected ECIs with a fixed number are continually optimized to predict the stable configurations for the different coverages of adatoms. The structure evolution of oxygen atoms on graphene is then investigated with the adaptive CE approach.

II. METHODOLOGY

A. Computational setup and model

All first-principles calculations were performed with the VASP package.⁴⁴ The exchange–correlation potential was described by the generalized gradient approximation functional of Perdew, Burke, and Ernzerhof (PBE).⁴⁵ The kinetic energy of the plane-wave basis was set to 550 eV. The geometry optimizations were stopped when the force on each ion was less than 0.01 eV/Å and the total energy converged to about 10^{-4} eV. A $3 \times 3 \times 1$ k-point sampling based on the Monkhorst–Pack scheme⁴⁶ was used for the rectangular supercell.

In the model, a (4×7) rectangular supercell of graphene was used, containing 112 C atoms and up to 19 oxygen atoms. During the calculations, only the possible bridge adsorption sites were considered because the bridge site is the most stable adsorption site for oxygen atoms.⁴⁷ There are several typical structures for a pair oxygen atoms adsorbing on graphene with a small distance between adsorbed oxygen atoms (<2.60 Å), as shown in Fig. 1(a). The typical structures are discussed for two reasons: imposing restriction on construction structures and preparing the discussion of distinguishing cluster function effectively in Secs. II B–II D. The A_1 - A_2 pair represents the pair configuration with two oxygen atoms occupying opposite sites of the same hexagon. B_1 - B_2 represents the configuration of two oxygen atoms on nearby hexagons. C_1 - C_2 represents the pair configuration with two oxygen atoms occupying the second nearest neighbor sites of the same hexagon. D_1 - D_2 corresponds to the unstable configuration with two oxygen atoms adsorbed at nearby bridge sites. In the calculations, the more preferable pair configurations were B_1 - B_2 and C_1 - C_2 , which were at least 0.25 eV lower in energy than any other pair configuration, such as those (not including themselves) in Fig. 1(b). The favored pair configurations impose restriction on constructing structures to reduce the number of the structures at coverage $(C_{112}O_x, 5 \leq x)$ in Sec. II C–II D.

To determine the most stable adsorption configuration, the adsorption energies E_{ad} of oxygen atoms on graphene were calculated. The adsorption energy is defined as follows:

$$E_{ad} = [E(GO_x) - \mu_G - x\mu_O]/x, \quad (1)$$

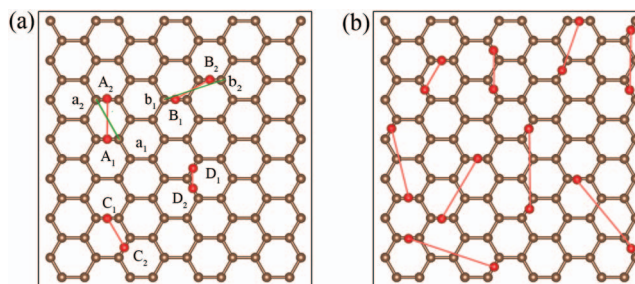


FIG. 1. (a) The four possible adsorption configurations for two oxygen atoms adsorbed on rectangular graphene with a relatively small distance (<2.6 Å) between adsorbed oxygen atoms, which are labeled as A_1 - A_2 , B_1 - B_2 , C_1 - C_2 , and D_1 - D_2 . The oxygen atoms are labeled with A, B, C, and D. The carbon atoms nearby the oxygen atoms are denoted by a and b. The distance parameters $[r_1, r_2]$ and $[r_1, r_3]$ can distinguish A_1 - A_2 and B_1 - B_2 , respectively. r_1 indicates the distance between A_1 and A_2 or B_1 and B_2 oxygen atoms, which are the same. r_2 indicates the distance between a_1 and a_2 , r_3 represents the distance between b_1 and b_2 nearby oxygen atoms. Here, the r_1 values are shown as red lines, and r_3 and r_2 are shown as green lines. (b) The final nine pair interactions selected in the calculations, as discussed in the adaptive CE method.

where $E(GO_x)$, μ_G , and μ_O are the energies of single sided graphene oxide, supercell graphene, and a single oxygen atom, respectively, and x is the number of oxygen atoms.

B. Cluster expansion

The CE approach was developed based on the well-known Ising Hamiltonian.^{48,49} The basic idea of CE is to expand the energy of any configuration into linear contributions of cluster functions,

$$\begin{aligned} E(\sigma) &= \sum_{\alpha} v_{\alpha} \langle \phi_{\alpha} \rangle \\ &= J_0 + \sum_i m_i J_i S_i(\sigma_i) + \sum_{i < j} m_{ij} J_{ij} S_i(\sigma_i) S_j(\sigma_j) \\ &\quad + \sum_{i < j < k} m_{ijk} J_{ijk} S_i(\sigma_i) S_j(\sigma_j) S_k(\sigma_k) + \cdots, \end{aligned} \quad (2)$$

where the indices i, j , and k run over all possible occupied bridge sites of graphene, E is the total energy of a configuration. ϕ_{α} is the cluster function, which includes cluster functions of single atoms, pairs of atoms, and so forth. m indicates the site number of the cluster function. The coefficient J_{α} in this expansion associated with every cluster function is called the effective cluster interaction (ECI), corresponding to the energy contribution of the correlative cluster function. By combining all of the contributions of the cluster functions in the configuration, the energy can be accurately obtained. $S_i(\sigma_i)$ is defined as 1 if site i is occupied by an oxygen atom, and 0 if it is unoccupied.

The main goal of the CE approach is to choose a finite number of cluster functions to reconstruct the physical properties of the system. In this work, the adsorption energy was used as the target function. The total energies of finite structures were first calculated by first-principles calculations. Unlike the cross-validation method,⁴⁹ the objective function for selecting the proper ECI in the case of cluster expansion of

the configuration energy is defined as follows:

$$F^2 = \sum_{i=1}^n K_i (E_i^{\text{re}} - E_i^{\text{ce}})^2. \quad (3)$$

Here, the index n is the total number of DFT calculated structures, K_i is the weight of a structure, which can be set as a constant, and E_i^{re} and E_i^{ce} are the corresponding energies of a specific structure from the DFT calculations (or experiment) and cluster expansion, respectively. By varying the number of ECIs to minimize F in Eq. (3), a set of ECIs is chosen. The set of ECIs with optimized values is used to predict the energies of all of the structures. In this work, scatter searching (SS)⁵⁰ was used to optimize Eq. (3) to obtain the global minimum value and values of a set of ECIs. SS is based on the premise that systematic designs and methods for creating new solutions afford significant benefits beyond those derived from recourse to randomization. A line search-based algorithm for solving high-dimensional continuous nonlinear optimization problems^{51,52} is included in the SS method to improve the local optimization accuracy. Detailed information of adaptive CE will be discussed below.

C. Construction of cluster functions and reduction of the number of structures

As mentioned above, the configurational energy is represented by the cluster functions. Thus, it is critical to accurately characterize the cluster functions to better represent any $E(\sigma)$ of a configuration. The total energy of a configuration can be represented using different cluster functions, which indicates the different contributions to the configurational energies. Whether the cluster functions effectively distinguish the similarity greatly affects the accuracy of the cluster expansion. Thus, the cluster function should be effectively described. When constructing the cluster function, the distance between two adsorption atoms is used to construct the pair cluster function. However, the distance itself cannot always effectively distinguish some pairs. We take the pair cluster function of oxygen atoms on bridge sites of graphene as an example. As shown in Fig. 1, several typical configurations of two oxygen atoms can exist on the graphene. The distances of A_1 - A_2 and B_1 - B_2 (r_1) are the same, although the two configurations are different. To distinguish the two different cluster functions, we considered the distance between carbon atoms closest to the oxygen atoms in the cluster function.

As shown in Fig. 1, r_2 represent the distance between carbon atoms a_1 and a_2 , and r_3 represents the distance between carbon atoms b_1 and b_2 . The cluster function A_1 - A_2 labeled with $[r_1, r_2]$ is different from B_1 - B_2 labeled with $[r_1, r_3]$. Similar to constructing cluster functions of pairs, the parameter sets to represent the cluster functions of triplets and quadruplets contain three and six parameters for the distance between occupying sites, respectively, and additional parameters for the distance between carbon atoms nearby the occupied sites are also included if the former parameters cannot distinguish the cluster function as pairs, as discussed above. The cluster function is characterized by a set of parameters including the relative distances of adatoms plus the distance

between nearby substrate atoms if necessary. To select the proper cluster functions for the next coverage, a cluster pool with all clusters within a distance cutoff was also constructed. We defined the distance cutoffs for cluster functions, that is, once a set of distance cutoffs $[R_2, R_3, R_4]$ are chosen, the corresponding cluster functions of pairs, triplets, and quadruplets with the largest distance parameters of adatoms r_2 ($r_2 < R_2$), r_3 ($r_3 < R_3$), and r_4 ($r_4 < R_4$) are also determined. In this work, the initial distance cutoffs for pairs, triplets, and quadruplets were selected as $[6 \text{ \AA}, 6 \text{ \AA}, 6 \text{ \AA}]$. See the supplementary material for detailed setups of cluster functions.⁵³

Well-characterized cluster functions are a prerequisite of the cluster expansion method. To reduce the computational cost, the similarity of structures is first checked to avoid repetition. The number list of the cluster function for a structure is compared with those of structures in the structure pool. If a number list of the cluster function is not found in the structure pool, the corresponding structure is kept, otherwise it is discarded. At relatively low coverages ($C_{112}\text{O}_x$, $1 \leq x \leq 4$), all configurations within the initial distance cutoffs were considered. At relatively high coverages ($C_{112}\text{O}_x$, $x \geq 5$), we only considered configurations at coverage $x \geq n$ by adding one extra oxygen atom to about 10^4 possible energy configurations at coverage $x \geq n-1$ when the extra oxygen atom formed at least one typical pair configuration (B_1 - B_2 or C_1 - C_2) bond with other oxygen atoms, considering that oxygen atoms prefer to cluster together.⁵⁴

D. Adaptive cluster expansion approach

Once the initial cluster functions with relatively large distance cutoffs of $[6 \text{ \AA}, 6 \text{ \AA}, 6 \text{ \AA}]$ for pairs, triplets, and quadruplets are chosen, the initial corresponding ECIs are obtained. However, it is also necessary to describe the physical properties by a finite number of ECIs. To verify the accuracy of the ECIs, the objective function, which defines the difference between the energies calculated by the cluster expansion method and first-principles calculation, as defined in Eq. (3), was used to check whether the configuration energies predicted by the selected ECIs agree with the first-principles energies. For this type of primary fitting, we started from oxygen adsorption on graphene at low coverage ($C_{112}\text{O}_x$, $1 \leq x \leq 7$). The objective function (F) was optimized by the SS method with different ECIs by changing the distance cutoffs from $[6 \text{ \AA}, 6 \text{ \AA}, 6 \text{ \AA}]$ to $[3.3 \text{ \AA}, 3.3 \text{ \AA}, 3.3 \text{ \AA}]$. In this case, the ECIs that lead to the smallest F were selected, while the predicted structure with the lowest energy was added to refit F again after the DFT calculation if the stable structure was not included in the last run. The loop was terminated when the structures with the lowest energies calculated by first-principles were well-reproduced by the selected ECIs.

Once the primary set of ECIs was selected at the low oxygen atom coverages ($C_{112}\text{O}_x$, $1 \leq x \leq 7$), the number of ECIs was fixed to predict the structural energies of higher coverages. However, the values of ECIs were gradually improved by adding adatoms into the system in this stage. For example, to predict the most stable configuration of eight adatoms on graphene, the initial structures of eight adatoms were constructed based on the $\sim 10^4$ possible energy structures in

the case of seven adatoms, and the corresponding configuration energies were calculated by the ECIs obtained in the seven adatom case. Similar to the primary fitting at the relatively low coverage, the most stable structures at coverages of $C_{112}O_x$ ($1 \leq x \leq 7$) as well as the new optimized values of the ECIs were obtained. In addition, if the most stable structure with a coverage of less than eight oxygen adatoms predicted by the CE method was obtained for the first time, the new structure was added to refit the ECIs again. The most stable configurations at the adsorption degrees ($C_{112}O_x$, $1 \leq x \leq 8$) were also updated. In this way, the most stable structures at each coverage were explored step-by-step.

III. APPLICATION OF ADAPTIVE CE TO INVESTIGATE STRUCTURE EVOLUTION OF GO

A. Construction of ECIs

As mentioned in Sec. I, it is difficult to predict the most stable configuration for adatoms on graphene because of the huge number of possible configurations.^{28,30} To solve this problem, the adaptive CE method was used to explore the oxidation process of graphene step-by-step for up to 19 oxygen atoms on a graphene sheet containing 112 carbon atoms.

The ECIs were first determined by minimizing the F value (Eq. (3)) for up to seven oxygen adatoms. In total, 25 clusters (ECIs) were obtained, which included the on-site atom, nine pair clusters, nine triplet clusters, and five quadruplet clusters in the CE fitting. The root-mean-square (rms), as defined by the objective function in Eq. (3), varied from 20 to 33 meV/adatom when the number of adatoms on the supercell of graphene changed from 7 to 13, suggesting the high reliability of the CE method. It should be noted that, as mentioned in Sec. II D, once the ECIs are chosen at the low coverage, the corresponding number of ECIs are fixed in the following steps, while the coefficients of J_α are continually optimized with increasing coverage ($8 \leq x \leq 13$). It should also be noted that both the number of ECIs and their values are fixed because of the extremely large number of the adsorption configurations to further explore the ground states of high coverage $C_{112}O_x$ ($14 \leq x \leq 19$).

B. $C_{112}O_x$ ($1 \leq x \leq 13$)

Once the ECIs were determined, the predicted energies of all adsorbed configurations were obtained, as shown in Fig. 2(a). With increasing oxygen adatom number, the curve of the adsorption energies per oxygen atom exhibits an upward parabola with the minimum near $C_{112}O_{11}$ (−3.15 eV/adatom). When the number of adsorbed atoms on graphene is greater than 11, the supersaturated oxygen causes an increase in the Coulomb repulsive force between the oxygen atoms and distortion of the substrate, which eventually leads to the increase of the adsorption energies for $C_{112}O_x$ ($x > 11$). As shown in Fig. 2(c), the fitted J_α values do not greatly change with increasing coverage from 7 to 13 adatoms. In addition, the convex hull (red line in Fig. 2(b)) connects all the stable (lowest) energy phases, which suggests that a total of nine stable phases ($C_{112}O_1$, $C_{112}O_2$, $C_{112}O_3$,

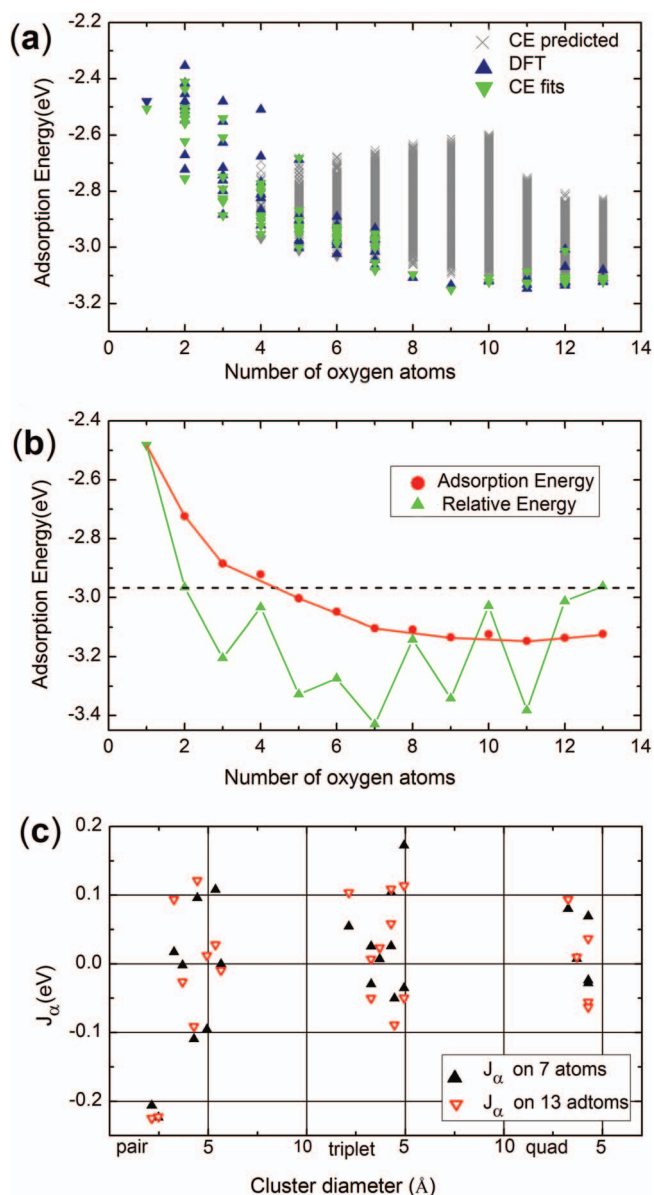


FIG. 2. (a) Calculated adsorption energies of $C_{112}O_x$ ($1 \leq x \leq 13$) as a function of the number of oxygen atoms. Here, the results predicted by CE are in grey, and the DFT results of selected structures and the corresponding results predicted by CE are blue and green, respectively. (b) Relative adsorption energy difference between x and $x - 1$ oxygen atoms ($\Delta E_A = E[x] - E[x - 1]$) (green) and the adsorption energy for the most stable configuration of each composition (red). The dashed line (black) denotes the adsorption energy of C_8O_1 predicted in another paper.²⁹ The structure of C_8O_1 ²⁹ is shown in the insert of Fig. 2(b). (c) Comparison of J_α values of the double, triple, and quadruplet for 7 and 13 adatoms, which were optimized with the adaptive CE approach. \blacktriangle and ∇ denote the J_α values for 7 and 13 adatoms, respectively.

$C_{112}O_5$, $C_{112}O_7$, $C_{112}O_9$, $C_{112}O_{11}$, and $C_{112}O_{13}$) exist in the whole graphene oxidation process ($1 \leq x \leq 13$). The corresponding most stable $C_{112}O_x$ ($1 \leq x \leq 13$) configurations for all coverages are shown in Fig. 3. Such results indicate that the oxygen atoms prefer to cluster together on graphene, which agrees well with previous first-principles calculations.^{28,30}

To determine whether the predicted ground states are the most stable configurations, we compared the adsorption energies with other reported structures. As reported in previous work, C_8O_1 is a rather stable configuration.²⁹ The adsorption

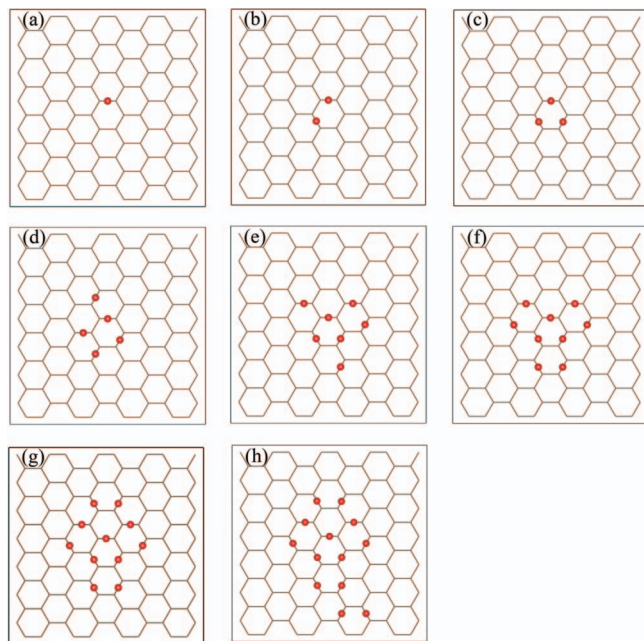


FIG. 3. Predicted energetically most favorable configurations of $C_{112}O_x$ ($1 < x < 14$): (a) $C_{112}O_1$, (b) $C_{112}O_2$, (c) $C_{112}O_3$, (d) $C_{112}O_5$, (e) $C_{112}O_7$, (f) $C_{112}O_9$, (g) $C_{112}O_{11}$, and (h) $C_{112}O_{13}$. Here, the graphene sheet is represented by the network and the red balls indicate the oxygen atoms.

energy per oxygen atom of the most stable structure of C_8O_1 is shown with the black dashed line in Fig. 2(b), which was previously predicted by the CE approach for up to 48 carbon graphene.²⁹ The adsorption energies per oxygen atom of the $C_{112}O_x$ configurations are larger than that of the C_8O_1 homogenous structure when the number of adsorbed oxygen atoms is greater than four. The corresponding energy difference between $C_{112}O_x$ and C_8O_1 varies from 0.03 eV/adatom ($x = 5$) to 0.18 eV/adatom ($x = 11$). Furthermore, when the number of adsorbed oxygen atoms becomes 14, the most stable configuration of $C_{112}O_{14}$ predicted by CE method, which has the similar ratio of oxygen to carbon atom to C_8O_1 , is also about 0.15 eV/adatom more stable than C_8O_1 . Such results clearly indicate that the inhomogeneous oxygen adsorption structures predicted in this study are more stable than the homogenous configuration of C_8O_1 , which further indicates that the oxygen atoms prefer to form inhomogeneous structures rather than homogenous structures. As shown in previous experimental and theoretical studies,^{13,28,30} the typical structure of GO is an amorphous phase,²⁴ and thus our results agree well with previous studies.

To understand the structural evolution during the graphene oxidation process, the structural characteristics of eight stable states for $C_{112}O_x$ ($1 \leq x \leq 13$) are shown in Fig. 3. For the adsorption of one oxygen atom on the bridge site of graphene (Fig. 3(a)), the adsorption energy was about -2.48 eV/adatom, which is consistent with a previous study.²⁸ When a second oxygen atom adsorbs on graphene, it prefers to occupy a nearby site to the first oxygen atom (see Fig. 3(b)), resulting in a larger negative adsorption energy (-2.72 eV/adatom) than that of a single oxygen atom on graphene. When a third oxygen atom adsorbs, the three oxygen atoms are prone to form a cluster on the graphene,

occupying three bridge sites in a hexagonal circle, as shown in Fig. 3(c). When first oxygen atom adsorption on graphene, the initial flat graphene becomes buckle one, and the carbon atoms interacting with oxygen move 0.24 Å out of the flat graphene, which suggests that the carbon atom form the sp^3 bonding. When the second oxygen atom adsorbs on the graphene, the corresponding carbon atoms interacting with oxygen becomes sp^3 bonding. The carbon atoms of two oxygen atoms stick out 0.47 Å from the flat graphene. The sp^3 carbon atoms prefer to cluster together, which should be the main reason that the oxygen atoms prefer to cluster on the graphene.

When the number of adsorbed oxygen atoms reaches five (see Fig. 3(d)), interestingly, the adsorption configuration of five adatoms does not follow the previous structure of three oxygen atoms by adding two atoms, while a phase transformation occurs as the number of oxygen atoms increases from three to five. Furthermore, when the number of oxygen atoms increases to seven, as illustrated in Fig. 3(e), the most stable configuration returns to the structural characteristics of the three adsorbed oxygen atom case. It should be noted that the adsorption of oxygen atoms is a continuous process along with energy minimization in the actual graphene oxidation process, and the phase change may not be easy to achieve. Therefore, the stable state of $C_{112}O_7$ is easier to produce from the $C_{112}O_3$ configuration by adding four adatoms than from the $C_{112}O_5$ configuration by adding two adatoms. The following graphene oxidation process, such as the $C_{112}O_9$, $C_{112}O_{11}$, and $C_{112}O_{13}$ configurations, shows a similar trend that the new configuration simply follows from the previous most stable configuration by adding extra oxygen atoms step-by-step (see Figs. 3(f)–3(h)). In this part of the discussion, we clearly uncovered the structural evolution characteristics during the graphene oxidation process. It is interesting to note that general characteristics of the oxygen atom adsorbed structures exist in the whole process. Moreover, the oxygen atoms tend to aggregate on the graphene rather than forming homogeneous or line configurations.

In our adaptive cluster expansion approach, as described in detail in Sec. II D, all of the possible coverage configurations ($5 \leq x \leq 13$) are constructed based on the previous low coverage configurations ($x \leq 4$). In this case, the new possible oxygen adsorption sites, which are selected to construct the stable structures of the high coverage, are limited to the previous predicted configurations, as mentioned in Sec. II C. Thus, it is essential to know whether the most stable structure with x oxygen atoms prefers to phase separate into two small stable structures with x_1 ($x_1 \leq x/2$) and x_2 ($x_2 = x - x_1$) oxygen atoms. Here, the distance between the two small separate clusters should be large enough to prevent interaction between the clusters. To answer this question, we considered all possible separated cases of $C_{112}O_x$ ($4 \leq x \leq 13$) configurations. The adsorption energy difference (ΔE) between the integrated cluster and the separated clusters can be calculated by the following equation:

$$\Delta E = E(x_1) + E(x_2) - E(x), \quad (4)$$

where $E(x_1)$ and $E(x_2)$ represent the adsorption energies of the separate clusters and $E(x)$ is the adsorption energy of the

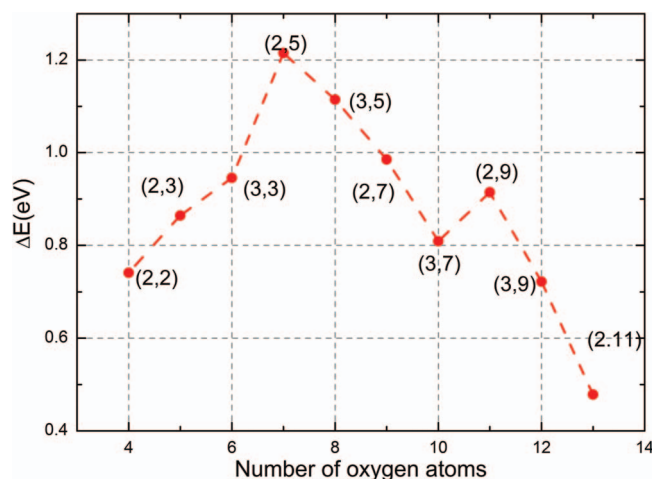


FIG. 4. Adsorption energy difference (ΔE) between the separated clusters ($C_{112}O_{x_1}$ and $C_{112}O_{x_2}$) and the integrated configuration $C_{112}O_x$ ($3 < x < 14$), as defined in Eq. (4). Here, (x_1, x_2) represent $C_{112}O_{x_1}$ and $C_{112}O_{x_2}$, and $x = x_1 + x_2$.

integrated configuration. The more positive the adsorption energy difference, the more stable the integrated $C_{112}O_x$ configurations.

In Fig. 4, all the selected most stable separate clusters of $C_{112}O_x$ ($4 \leq x \leq 13$) are in line with the predicted stable configurations located on the convex hull (see Fig. 2(a)). For example, the most stable separated combination of $C_{112}O_{10}$ was selected to consist of two small clusters with seven and three oxygen adatoms. This is somewhat expected because of the energy advantage of these convex-hull structures. It can be seen that all the integrated $C_{112}O_x$ structures are more stable than the separated small clusters, with energy differences ranging from 0.41 to 1.20 eV. This suggests that for a given number of oxygen atoms ($4 \leq x \leq 13$), the oxygen atoms prefer to form a large cluster rather than two smaller clusters on graphene. In addition, such results further suggest the reliability of the $C_{112}O_x$ ($4 \leq x \leq 13$) stable structures, which were predicted in the prior CE steps.

C. $C_{112}O_x$ ($14 \leq x \leq 19$)

We have already explored the structural evolution of the graphene oxidation process for up to 13 adsorbed oxygen atoms. However, it is computationally expensive to predict all configurations by the CE approach combined with the first-principles approach for more than 13 adsorbed atoms because of the extremely large number of possible oxygen adsorption configurations. To solve this problem, we used the ECIs constructed for the case of 13 adsorbed oxygen atoms to reproduce the adsorption energies of all possible configurations for more than 13 adsorbed oxygen atoms. This is feasible because the oxygen atoms are prone to cluster on graphene, and the interaction of oxygen atoms mainly depends on short-range effects, which are mostly included in the cases with less than 13 adsorbed atoms. Thus, the constructed ECIs can be further used to describe the energies of $C_{112}O_x$ ($x > 13$) configurations. To verify the reliability of the ECIs for high oxygen coverages of $C_{112}O_x$ ($x > 13$), the energies of the most

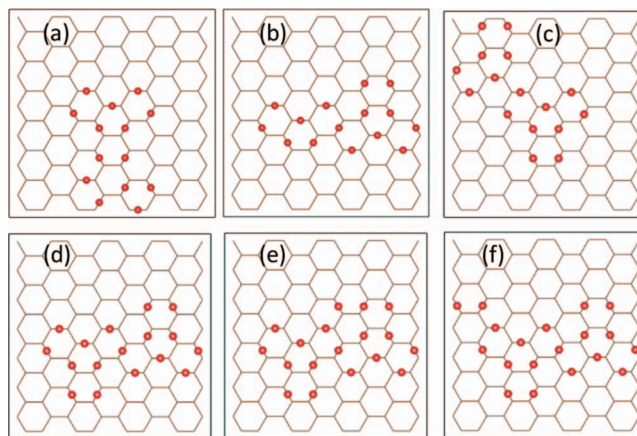


FIG. 5. Most stable configurations of $C_{112}O_x$ ($14 \leq x \leq 19$) predicted by the CE method: (a) $C_{112}O_{14}$, (b) $C_{112}O_{15}$, (c) $C_{112}O_{16}$, (d) $C_{112}O_{17}$, (e) $C_{112}O_{18}$, and (f) $C_{112}O_{19}$. Here, the graphene sheet is represented by the network and the red balls indicate the oxygen atoms.

stable $C_{112}O_{14}$ configurations predicted by the ECIs were compared with DFT calculation results. The energy difference between the predicted energies and DFT calculated energies of the most stable $C_{112}O_{14}$ configurations were within 9 meV/adatom, indicating the high reliability of the CE calculations. The results indicate that the ECIs obtained in the case of 13 adsorbed atoms can be used to explore the stable configuration at high oxygen coverages of $C_{112}O_x$ ($x > 13$).

The predicted most stable $C_{112}O_x$ ($14 \leq x \leq 19$) configurations are shown in Fig. 5. It is interesting to note that the oxygen atoms in the high coverage cases retain the characteristic of an inhomogeneous distribution on graphene. The most stable configurations of the high oxygen coverages would be inclined to form two (or several) lower coverage parts, and these parts are shown to be linked by one or several oxygen adatoms. For example, the most stable configuration of $C_{112}O_{17}$ can be regarded as being composed by two parts containing nine oxygen adatoms, as shown in Fig. 5(d). There is a mutual oxygen atom between these two parts, and this atom acts as a “bridge” to link two “islands.” It can be inferred that the large number of oxygen atoms would prefer to form several medium-sized islands on a large enough graphene substrate. With further increasing coverage, the oxygen atoms have no choice but to occupy appropriate sites between these islands to form low energy configurations.

D. Discussion of the structure evolution of oxygen atoms on graphene

To further understand the intrinsic mechanism of structure evolution, the relationship between the structural characteristics and the adsorption energies of the $C_{112}O_x$ ($1 \leq x \leq 19$) configurations was investigated. It should be noted that oxygen adsorption on one single side of graphene induces large structural corrugation because of the strain induced by oxygen adatoms on one side of graphene, while oxygen adsorption on both side of graphene induces a relative smaller structural corrugation. In this work, we only examine the structure of oxygen adsorption on one side of graphene.

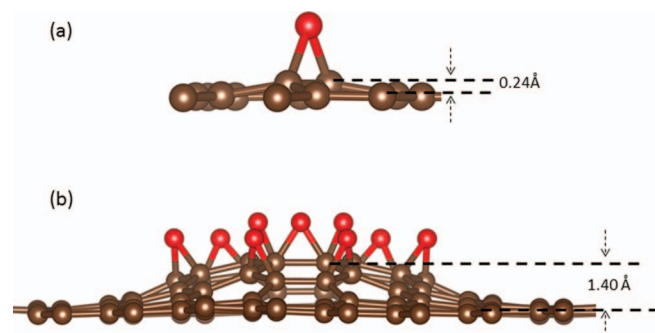


FIG. 6. (a) Side view of the most stable adsorption configurations of oxygen atoms on one side of graphene: (a) one oxygen atom and (b) nine oxygen atoms. The buckling distances of the graphene because of oxygen adsorption are labeled. Here, the red balls represent oxygen atoms and the brown balls represent carbon atoms.

The substrate carbon atoms below the oxygen atom cluster are greatly distorted and pulled towards the oxygen atoms to form corrugation. As well as chemical bonding between oxygen and carbon atoms, distortion also greatly affects the total energy of the system. When the first oxygen atom adsorbs on graphene, the carbon atoms below the adsorbed oxygen atoms are distorted, and the carbon atom also moves out of the plane of the graphene sheet towards the oxygen atom, which results in buckling of 0.24 Å above the plane of graphene (see Fig. 6(a)). The reason for the out-of-plane buckling of the graphene sheet is mainly the electronic structure of the graphene changing from a planar sp^2 -hybridized to a distorted sp^3 -hybridized geometry.

The amount of distortion increased with further addition of oxygen atoms. For example, in the case of the $C_{112}O_9$ configuration, the buckling increased to 1.40 Å (see Fig. 6(b)). It should be noted that such structural deformation results in energy increase of the graphene substrate. The newly generated C–O bonding interactions, as well as the adsorption of the oxygen cluster on the graphene sheet, can effectively offset the energy increase caused by the structural deformation, which could lead to a negative adsorption energy. At the initial stage of the graphene oxidation process, the number of oxygen atoms gradually increases from 1 to 11, and at the low coverage the structural change may not be strong enough to affect the adsorption energies. Nonetheless, with further adsorption of oxygen atoms, the energy change of $C_{112}O_x$ ($14 \leq x \leq 19$) is mainly dominated by the large structural distortion, leading to higher adsorption energies. To lower the distortion, the oxygen atoms have to form several bridge-linked islands to lower the distortion because of the repulsion effects of the oxygen atoms. The formation of several islands of oxygen adatoms agrees with previous work,⁵⁵ which suggested that an initial homogenous GO phase may separate into an inhomogeneous phase composed of several islands. Because oxygen–oxygen gathering behavior can lower the energy, the bridge atoms not only help link the islands, but also help to lower the energy. The competition between the distortion of graphene substrate and the interaction of oxygen atoms determines the most stable configuration of GO for each coverage. From the above discussion, the adsorption energy minimum is near the $C_{112}O_{11}$ configuration, and bridge-linked is-

land structures are present at high oxygen coverages ($C_{112}O_x$, $14 \leq x \leq 19$).

IV. CONCLUSIONS

In summary, an adaptive CE method was used to predict the surface adsorption and growth progress. Checking for structural similarity was performed first to reduce the number of structures. To effectively reduce the computational cost while maintaining the accuracy, the suitable effective cluster interaction (ECIs) parameters, as well as the stable configurations of low oxygen coverages ($C_{112}O_x$, $1 \leq x \leq 7$) were determined. Once the ECIs were chosen for low coverages, the number of ECIs were then fixed and their values were changed step-by-step to predict the stable configurations of high coverages ($C_{112}O_x$, $8 \leq x \leq 13$) with updating the stable configurations of coverages ($C_{112}O_y$, $y \leq x$). Finally, the ECIs obtained from the 13 adatom case were used to predict the stable configurations at high coverages ($C_{112}O_x$, $14 \leq x \leq 19$) with both the number of ECIs and their values unchanged. The results successfully uncovered the structural evolution of the single sided graphene oxidation process and gave the stable configurations at different oxygen atom coverages. It was shown that the oxygen atoms preferred to arrange inhomogeneously rather than homogeneously or aggregating together, which is consistent with previous work. More importantly, general characteristics exist in the whole graphene oxidation process. For high oxygen coverages ($C_{112}O_x$, $14 \leq x \leq 19$), the stable configurations tended to be formed by two (or several) stable lower coverage parts linking by several oxygen adatoms. This can be explained by the synergetic effect of the interactions of oxygen atoms and the distortion of graphene substrate. It should be noted that, as a targeted method, the adaptive CE method can also be used for other surface adsorption and growth problems.

ACKNOWLEDGMENTS

This work was supported by the National Natural Science Foundation of China (Grant No. 51222212), the CAEP foundation (Grant No. 2012B0302052), and the MOST of China (973 Project, Grant No. 2011CB922200). The computations supports from Informalization Construction Project of Chinese Academy of Sciences during the 11th Five-Year Plan Period (Grant No. INFO-115-B01) are also highly acknowledged.

¹C. Lee, X. Wei, J. W. Kysar, and J. Hone, *Science* **321**(5887), 385–388 (2008).

²K. S. Novoselov, A. K. Geim, S. V. Morozov, D. Jiang, Y. Zhang, S. V. Dubonos, I. V. Grigorieva, and A. A. Firsov, *Science* **306**(5696), 666–669 (2004).

³M. I. Katsnelson, K. S. Novoselov, and A. K. Geim, *Nat. Phys.* **2**(9), 620–625 (2006).

⁴A. K. Geim and K. S. Novoselov, *Nat. Mater.* **6**(3), 183–191 (2007).

⁵A. A. Balandin, *Nat. Mater.* **10**(8), 569–581 (2011).

⁶X. Gao, Z. Wei, V. Meunier, Y. Sun, and S. B. Zhang, *Chem. Phys. Lett.* **555**, 1–6 (2013).

⁷P. P. Shinde and V. Kumar, *Phys. Rev. B* **84**(12), 125401 (2011).

⁸T. Ohta, A. Bostwick, T. Seyller, K. Horn, and E. Rotenberg, *Science* **313**(5789), 951–954 (2006).

- ⁹M. Y. Han, B. Özyilmaz, Y. Zhang, and P. Kim, *Phys. Rev. Lett.* **98**(20), 206805 (2007).
- ¹⁰L. Ci, L. Song, C. Jin, D. Jariwala, D. Wu, Y. Li, A. Srivastava, Z. F. Wang, K. Storr, L. Balicas, F. Liu, and P. M. Ajayan, *Nat. Mater.* **9**(5), 430–435 (2010).
- ¹¹D. C. Elias, R. R. Nair, T. M. G. Mohiuddin, S. V. Morozov, P. Blake, M. P. Halsall, A. C. Ferrari, D. W. Boukhvalov, M. I. Katsnelson, A. K. Geim, and K. S. Novoselov, *Science* **323**(5914), 610–613 (2009).
- ¹²K. P. Loh, Q. Bao, G. Eda, and M. Chhowalla, *Nat. Chem.* **2**(12), 1015–1024 (2010).
- ¹³Y. Zhu, S. Murali, W. Cai, X. Li, J. W. Suk, J. R. Potts, and R. S. Ruoff, *Adv. Mater.* **22**(35), 3906–3924 (2010).
- ¹⁴X.-H. Zha, R.-Q. Zhang, and Z. Lin, *J. Chem. Phys.* **141**(6), 064705 (2014).
- ¹⁵L. Liu, J. Zhang, J. Zhao, and F. Liu, *Nanoscale* **4**(19), 5910–5916 (2012).
- ¹⁶A. Du, Y. H. Ng, N. J. Bell, Z. Zhu, R. Amal, and S. C. Smith, *J. Phys. Chem. Lett.* **2**(8), 894–899 (2011).
- ¹⁷D. W. Boukhvalov and M. I. Katsnelson, *J. Am. Chem. Soc.* **130**(32), 10697–10701 (2008).
- ¹⁸K.-Y. Lian, Y.-F. Ji, X.-F. Li, M.-X. Jin, D.-J. Ding, and Y. Luo, *J. Phys. Chem. C* **117**(12), 6049–6054 (2013).
- ¹⁹T. Nakajima and Y. Matsuo, *Carbon* **32**(3), 469–475 (1994).
- ²⁰W. Gao, L. B. Alemany, L. J. Ci, and P. M. Ajayan, *Nat. Chem.* **1**(5), 403–408 (2009).
- ²¹S. Park and R. S. Ruoff, *Nat. Nano* **4**(4), 217–224 (2009).
- ²²D. Pacilé, J. C. Meyer, A. Fraile Rodríguez, M. Papagno, C. Gómez-Navarro, R. S. Sundaram, M. Burghard, K. Kern, C. Carbone, and U. Kaiser, *Carbon* **49**(3), 966–972 (2011).
- ²³K. Krishnamoorthy, M. Veerapandian, K. Yun, and S. J. Kim, *Carbon* **53**, 38–49 (2013).
- ²⁴K. Erickson, R. Erni, Z. Lee, N. Alem, W. Gannett, and A. Zettl, *Adv. Mater.* **22**(40), 4467–4472 (2010).
- ²⁵P. Zhu, B. G. Sumpter, and V. Meunier, *J. Phys. Chem. C* **117**(16), 8276–8281 (2013).
- ²⁶L. Wang, T. Maxisch, and G. Ceder, *Phys. Rev. B* **73**(19), 195107 (2006).
- ²⁷R. Lahaye, H. Jeong, C. Park, and Y. Lee, *Phys. Rev. B* **79**(12), 125435 (2009).
- ²⁸M. Topsakal and S. Ciraci, *Phys. Rev. B* **86**(20), 205402 (2012).
- ²⁹B. Huang, H. Xiang, Q. Xu, and S.-H. Wei, *Phys. Rev. Lett.* **110**(8), 085501 (2013).
- ³⁰M.-T. Nguyen, R. Erni, and D. Passerone, *Phys. Rev. B* **86**(11), 115406 (2012).
- ³¹Z. Xu and K. Xue, *Nanotechnology* **21**(4), 045704 (2010).
- ³²N. Lu, D. Yin, Z. Li, and J. Yang, *J. Phys. Chem. C* **115**(24), 11991–11995 (2011).
- ³³W. Scholz and H. P. Boehm, *Z. Anorg. Allg. Chem.* **369**(3–6), 327 (1969).
- ³⁴H. C. Schniepp, K. N. Kudin, J. L. Li, R. K. Prud'homme, R. Car, D. A. Saville, and I. A. Aksay, *ACS Nano* **2**(12), 2577–2584 (2008).
- ³⁵J. A. Yan, L. D. Xian, and M. Y. Chou, *Phys. Rev. Lett.* **103**(8), 086802 (2009).
- ³⁶J. L. Li, K. N. Kudin, M. J. McAllister, R. K. Prud'homme, I. A. Aksay, and R. Car, *Phys. Rev. Lett.* **96**(17), 176101 (2006).
- ³⁷A. Lerf, H. Y. He, M. Forster, and J. Klinowski, *J. Phys. Chem. B* **102**(23), 4477–4482 (1998).
- ³⁸T. Nakajima, A. Mabuchi, and R. Hagiwara, *Carbon* **26**(3), 357–361 (1988).
- ³⁹Y. Wang, J. Lv, L. Zhu, and Y. Ma, *Phys. Rev. B* **82**(9), 094116 (2010).
- ⁴⁰S. Q. Wu, M. Ji, C. Z. Wang, M. C. Nguyen, X. Zhao, K. Umemoto, R. M. Wentzcovitch, and K. M. Ho, *J. Phys.: Condens. Matter* **26**(3), 035402 (2014).
- ⁴¹X. Zhao, M. C. Nguyen, W. Y. Zhang, C. Z. Wang, M. J. Kramer, D. J. Sellmyer, X. Z. Li, F. Zhang, L. Q. Ke, V. P. Antropov, and K. M. Ho, *Phys. Rev. Lett.* **112**(4), 045502 (2014).
- ⁴²D. Wang, L.-M. Liu, S.-J. Zhao, B.-H. Li, H. Liu, and X.-F. Lang, *Phys. Chem. Chem. Phys.* **15**(23), 9075–9083 (2013).
- ⁴³L.-C. Xu, R.-Z. Wang, M.-S. Miao, X.-L. Wei, Y.-P. Chen, H. Yan, W.-M. Lau, L.-M. Liu, and Y.-M. Ma, *Nanoscale* **6**(2), 1113–1118 (2014).
- ⁴⁴G. Kresse and J. Furthmüller, *Comput. Mater. Sci.* **6**(1), 15–50 (1996).
- ⁴⁵J. P. Perdew, K. Burke, and M. Ernzerhof, *Phys. Rev. Lett.* **77**(18), 3865–3868 (1996).
- ⁴⁶H. J. Monkhorst and J. D. Pack, *Phys. Rev. B* **13**(12), 5188–5192 (1976).
- ⁴⁷K. Nakada and A. Ishii, *Solid State Commun.* **151**(1), 13–16 (2011).
- ⁴⁸Y. Zhang, V. Blum, and K. Reuter, *Phys. Rev. B* **75**(23), 235406 (2007).
- ⁴⁹L. G. Ferreira, S.-H. Wei, and A. Zunger, *Phys. Rev. B* **40**(5), 3197–3231 (1989).
- ⁵⁰F. Glover, in *Artificial Evolution*, edited by J.-K. Hao, E. Lutton, E. Ronald, M. Schoenauer, and D. Snyers (Springer, Berlin, 1998), Vol. 1363, pp. 1–51.
- ⁵¹V. Gardeux, R. Chelouah, P. Siarry, and F. Glover, in *Proceedings of the 2009 Ninth International Conference on Intelligent Systems Design and Applications* (IEEE Computer Society, 2009), pp. 1096–1101.
- ⁵²V. Gardeux, R. Chelouah, P. Siarry, and F. Glover, *Soft Comput.* **15**(11), 2275–2285 (2011).
- ⁵³See supplementary material at <http://dx.doi.org/10.1063/1.4903310> for detailed setups of cluster functions.
- ⁵⁴L.-M. Liu, R. Car, A. Selloni, D. M. Dabbs, I. A. Aksay, and R. A. Yetter, *J. Am. Chem. Soc.* **134**(46), 19011–19016 (2012).
- ⁵⁵L. Wang, Y. Y. Sun, K. Lee, D. West, Z. F. Chen, J. J. Zhao, and S. B. Zhang, *Phys. Rev. B* **82**(16), 161406 (2010).